ACS SENSORS

pubs.acs.org/acssensors

Article

Handheld Purification-Free Nucleic Acid Testing Device for Point-of-Need Detection of Malaria from Whole Blood

Aneesh Kshirsagar, Gihoon Choi, Vishaka Santosh, Tara Harvey, Robert Cory Bernhards, and Weihua Guan*

Cite This: *ACS Sens.* 2023, 8, 673−683

Read Online

ACCESS | Metrics & More | Article Recommendations | Supporting Information

ABSTRACT: World Health Organization's aim to eliminate malaria from developing/resource-limited economies requires easy access to low-cost, highly sensitive, and specific screening. We present a handheld nucleic acid testing device with on-chip automated sample preparation to detect malaria (*Plasmodium falciparum*) infection from a whole blood sample as a feasibility study. We used a simple two-reagent-based purification-free protocol to prepare the whole blood sample on a piezo pump pressure-driven microfluidic cartridge. The cartridge includes a unique mixing chamber for sample preparation and metering structures to dispense a predetermined volume of the sample lysate mixture into four chambers containing a reaction mix. The parasite genomic DNA concentration can be estimated by monitoring the fluorescence generated from the loop-mediated isothermal amplification reaction in real time. We achieved a sensitivity of ∼0.42 parasite/μL of whole blood, sufficient for detecting asymptomatic malaria parasite carriers.

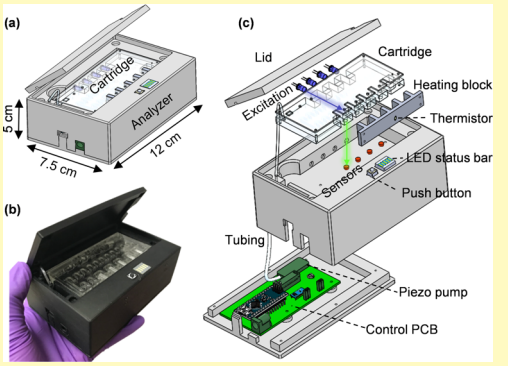

KEYWORDS: *purification-free, nucleic acid testing (NAT), loop-mediated isothermal amplification (LAMP), malaria, microfluidics, point-of-need*

Malaria parasites transmitted via female *Anopheles* mosquito bites can cause high fevers, shaking chills, and flu-like symptoms. Four main kinds of parasites are *Plasmodium falciparum(Pf)*, *Plasmodium vivax(Pv)*, *Plasmodium ovale(Po)*, and *Plasmodium malariae(Pm)*, of which *Pf* is considered the deadliest. World Health Organization (WHO) reported that 241 million clinical malaria cases occurred in 2020, resulting in 627,000 deaths, a high portion from Africa.[1] The complex disease poses challenges due to the highly adaptable nature of the vector and parasites involved. The different species of the *Plasmodium* genus respond to medications differently and develop drug resistance in different mechanisms, which makes the development of a fool-proof vaccine difficult.[2] Timely treatment of an infection with correct species-specific drugs can clear the patient's body of all parasites.[3] Hence, to enable prompt diagnosis and control of the spread, specific, sensitive, rapid, accurate, and low-cost tests that can be performed at the point-of-need (PON) are imperative.

Conventional malaria rapid diagnostic tests (RDTs) typically target a specific protein, for example, histidine-rich protein II (HRP-II) or lactate dehydrogenase (LDH), with a typical detection limit of 100−200 parasites/μL.[4] NxTek Eliminate Malaria *Pf* from Abbott,[5] FalciVax-Rapid test for malaria *Pv/Pf* from Zephyr Biomedicals,[6] and Paracheck *Pf* from Orchid[7] are just some of the currently available RDTs. Lee et al. suggest that false-positive results due to nonspecific biomolecules reacting with the test antigens limit the effective use of RDTs.[8] Additionally, HRP-II- and/or III-deleted *Pf* parasites have emerged in several African and South American countries, as well as India,[9] presenting challenges to malaria control and elimination efforts. Feleke et al. estimated that HRP-II-based RDTs would miss 9.7% *Pf* malaria cases owing to HRP-II deletion.[10] Thus, on the one hand, RDTs that exclusively rely on HRP-II detection may completely miss the infection (i.e., false negative), leading to further spread of this mutated parasite, and, on the other hand, combination RDTs that use HRP-II and LDH may misclassify the infection as non-*Pf*, leading to incorrect diagnosis and treatment. Moreover, RDTs fall short of measuring the degree of infection and often need to be followed up by microscopic examination by experts who can typically detect an infection with more than 50 parasites/μL.[11] Malaria detection using microscopic evaluation remains the gold standard. Briefly, a blood specimen collected from the patient is spread as a thick or thin blood smear, stained with a Romanowsky stain (most often Giemsa), and examined with a

Received: October 4, 2022
Accepted: January 11, 2023
Published: January 25, 2023

100× oil-immersion objective.[12] Visual criteria are used to detect the presence of malaria parasites in the thick smear, followed by species identification and quantitation of parasitemia in the thin smear. Berzosa et al. report that among 1724 samples tested by microscopy, 335 (19.4%) were false negatives.[13] Thus, the accuracy of microscopic detection relies heavily on the technician's skill and quality control. Auxiliary clinics in remote rural settings seldom offer advanced microscopy setups delaying the precise detection or even misdiagnosing of the infection resulting in negligent treatment or excessive use of antimalarial drugs, which invariably contributes to malaria morbidity and the development of resistance.[14] In general, microscopy and RDTs in field settings are prone to false negatives due to low parasitemia, which may result in undetected asymptomatic infections. However, timely treatment can completely cure a malaria infection if diagnosed when parasitemia concentration is low. In addition, malaria elimination efforts also require identifying these asymptomatic carriers, which tests with significantly improved detection limits will facilitate.

Nucleic acid tests (NATs) can achieve a limit of detection as low as 0.1 parasite/μL for malaria,[15] making them strong candidates to replace microscopic detection of malaria parasites. Since the first application of polymerase chain reaction (PCR) for *Plasmodium* detection,[16] numerous efforts have been made to develop nested[17] and multiplexed PCR[18] tests warranting its widespread use for identifying infections. However, PCR often requires bulky thermal cyclers, costly logistics, skilled technicians, and purified samples, limiting its use at the PON. Loop-mediated isothermal amplification (LAMP) is a promising molecular replication technique that requires only a constant temperature between 55 and 65 °C and can be easily implemented in a PON format due to its simplicity and robustness.[19,20] Loopamp malaria (Pan/*Pf*) detection kit (Eiken Chemical Company, Tokyo, Japan)[21,22] and Illumigene malaria LAMP assay (Meridian Bioscience, Cincinnati, OH)[23,24] are examples of commercially available LAMP kits.

Our previous work reported the development of a palm-sized instrument capable of quadruplex parallel LAMP reactions from sample to answer on a single closed microfluidic disc using a magnetic bead-based extraction protocol.[25] We achieved a detection limit of 0.5 parasite/μL from the whole blood sample within 50 min. Xu et al. reported a paper-based origami device that vertically processed the blood sample to extract, amplify (using LAMP), and detect specific malaria sequences on a lateral flow detection platform.[26] Thus, most microfluidics-based platforms that have been developed fall into three categories: pump-based, paper-based, and centrifugal-force-based. Paper-based devices that rely on capillary action for sample transport often demonstrate variability in capillary transport due to surface evaporation sacrificing adequate sensitivity and accurate quantitation.[27] Lab-on-a-disk platforms that rely on centrifugal force to drive liquid to the desired location in the microfluidic disc are often energy hungry. Pump-based approaches have traditionally used benchtop syringe pumps along with multiple tubes and complex valving, making the system bulky and difficult to be integrated for PON applications.

So far, most PON tests require elaborate sample preparation steps such as cell lysis, DNA/RNA isolation, purification, washing, concentration, and elution that may be performed using magnetic beads,[28] paper-based spin columns,[29] or salt precipitation.[30] QIAamp DNA Blood Mini Kit (Qiagen, Hilden, Germany) and PURE (Eiken Chemical Company, Tokyo, Japan)[31] are examples of commercially available extraction kits. Mens et al. presented a direct-on-blood PCR test that adds blood directly to the PCR mix.[32] The end point result was visualized using a nucleic acid lateral flow immunoassay (NALFIA). Thus, although there are multiple examples of commercialized PCR and LAMP assays based on extracted and purified DNA from infected whole blood, their adoption for direct-on-blood tests remains complicated because contamination from human carryover components, such as proteins, lipids, hemoglobin, hematin, and immunoglobulin G, can cause interference in optical detection methods and inhibit amplification.[33] As a result, malaria DNA extraction and purification steps are often required before downstream processing. A test that can be done with whole blood but without complicated sample preparation steps while limiting the inhibitory effects is highly desirable for PON testing (PONT).

This work presents an automated nucleic acid testing device relying on the unique reagent-based Arcis sample preparation chemistry and a continuous flow microfluidic chip assay that can run direct-on-blood LAMP and demonstrates reliable and sensitive malaria detection. This PON testing platform has a continuous flow pressure-driven on-chip sample preparation protocol to combine the blood lysate with Arcis reagents utilizing an ellipsoid-shaped structure coupled with the contact angle hysteresis of a hydrophilic surface and vertically dispense a predetermined mixture volume into four chambers with a preloaded LAMP mix utilizing a semicircular metering structure. It also has built-in optics to monitor the fluorescence emitted by the LAMP reaction in real time and can reliably detect the presence of 0.42 parasite/μL of malaria (*Pf*) in a whole human blood sample.

RESULTS AND DISCUSSION

Validation of the Purification-Free Sample Preparation. Nucleic acid (NA) extraction is the first step in molecular diagnosis and is crucial to ensure the results are reliable and clinically relevant.[34] It has the following objectives: to ensure the integrity of the primary structure of nucleic acid molecules is preserved, to exclude other molecular contaminants, and to optimize yield.[35] It is also essential to evaluate whether the quality of sample preparation varies with the concentration of the infection-causing agent since it is desirable to have highly efficient NA extraction to detect a sample with low NA concentration. We use the Arcis Sample Prep Kit, a commercial NA extraction kit from Arcis Biotechnology, U.K., consisting of two reagents. Arcis Reagent 1 (Arcis 1 hereafter) works as a lysis agent to release NAs in the blood, chelate them, and stabilize the DNA. Arcis Reagent 2 (Arcis 2 hereafter) removes the NA chelation and relaxes the DNA while binding any PCR or LAMP inhibitors present in the blood that may prevent DNA amplification. Although Arcis 2 is a proprietary mixture, the key components may include additives such as bovine serum albumin (BSA), dimethyl sulfoxide (DMSO), and T4 bacteriophage gene 32 product (gp32) that reportedly improve DNA−polymerase interaction and benefit PCR amplification.[36] Together, these allow blood to be processed for a molecular diagnostic test in approximately 3 min without any DNA isolation or purification steps. Since the protocol does not isolate the DNA extracted from whole blood, certain other blood components may be carried over to downstream analyses, making spectrophotometric approaches such as nanodrop inaccurate in quantifying the extracted DNA. We performed *Pf* DNA extraction from whole blood and investigated the

https://doi.org/10.1021/acssensors.2c02169
ACS Sens. 2023, 8, 673−683

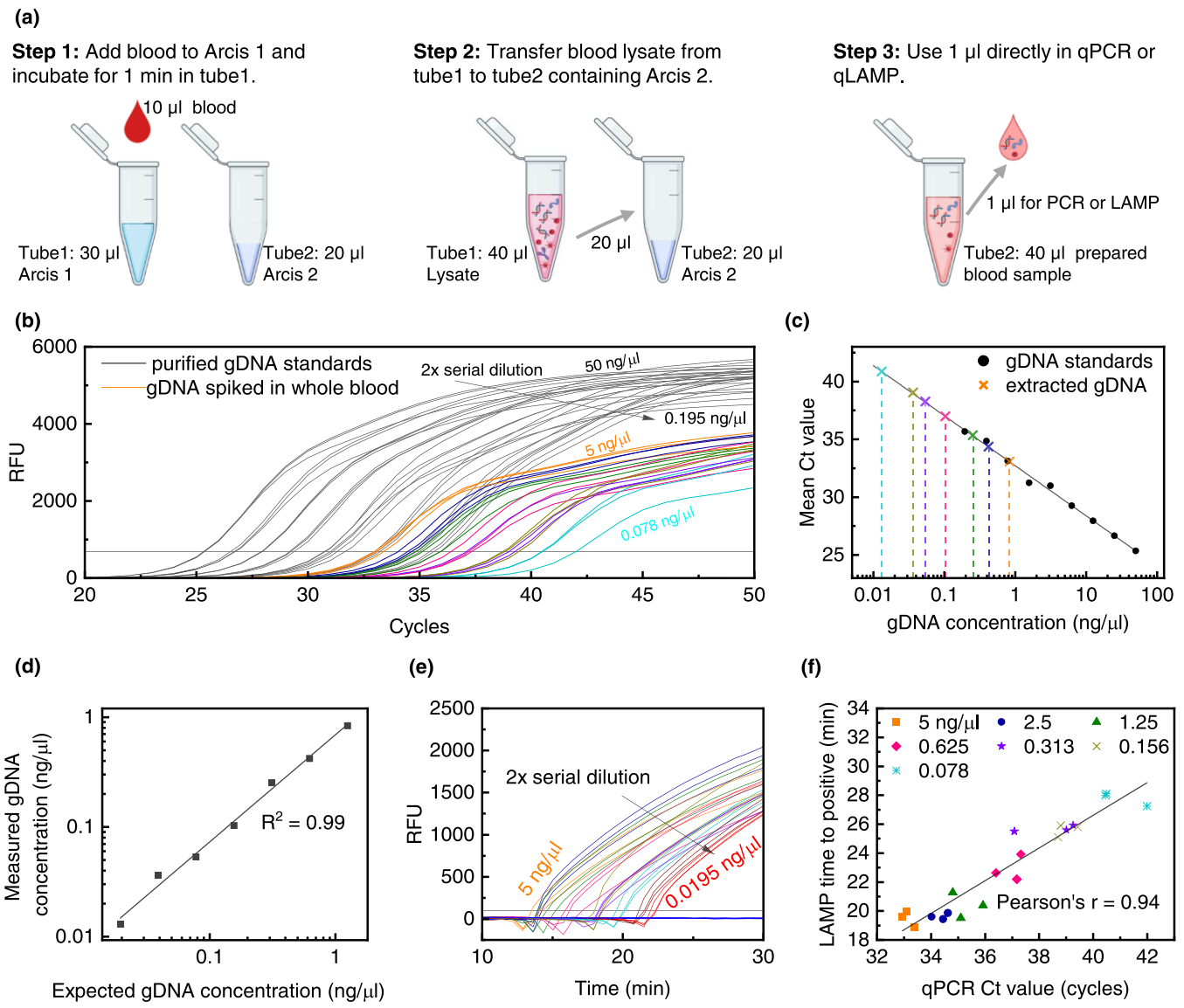

Figure 1. (a) Extraction and purification-free Arcis sample preparation protocol performed in tubes. Step 1: add *Pf*-positive blood to Arcis 1 (1:3 v/v), step 2: add blood lysate from step 1 to Arcis 2 (1:1 v/v), and step 3: use 1 μL of the mixture from step 2 in a 25 μL amplification reaction. (b) Black curves represent the qPCR amplification curves (triplicates) with 1 μL of 2-fold serially diluted *Pf* gDNA (stock concentration 50 ng/μL) as standards in a 25 μL total reaction volume. Ct values are used to generate the qPCR standard curve in panel (c). Colored curves represent the qPCR amplification curves (triplicates) with 1 μL of Arcis-prepared *Pf* gDNA-spiked whole blood. (c) qPCR standard curve. Black circles represent mean Ct values for gDNA samples and are used to construct the standard curve. Colored crosses represent mean Ct values for prepared spiked whole blood samples and are used to determine the resulting gDNA concentration after "extraction" or sample preparation. (d) Measured gDNA concentration versus expected gDNA concentration in whole blood as a result of dilution. Blood samples spiked with 0.039 and 0.019 ng/μL gDNA are not amplified within 55 cycles due to dilution. (e) LAMP curves (triplicates) for Arcis-prepared *Pf* gDNA-spiked whole blood samples, identical to those used in panel (b). Blood samples spiked with 0.039 and 0.019 ng/μL gDNA are amplified by the LAMP assay. (f) Correlation between LAMP times to positive and qPCR cycle thresholds for Arcis-prepared *Pf* gDNA-spiked whole blood samples.

extraction efficiency by performing downstream PCR analysis based on a standard qPCR curve.

A contrived blood sample was prepared by spiking 9 μL of negative whole blood with 1 μL of *Pf* gDNA (3D7, stock concentration 50 ng/μL). Nine such blood samples were prepared by serially diluting the gDNA 2-fold. Figure 1a outlines the Arcis sample preparation steps performed on the contrived blood samples manually in microcentrifuge tubes. Each 10 μL of blood sample was subjected to DNA extraction by incubating it with 30 μL of Arcis 1 for 1 min and then mixing 20 μL of the resulting lysate with 20 μL of Arcis 2. Figure 1b shows the qPCR (reaction volume: 25 μL) amplification curves for 1 μL of 2-fold serially diluted purified gDNA (black) and 1 μL of processed contrived blood (colored) as samples. Average Ct values of the gDNA triplicates were used to generate a standard qPCR curve by plotting the Ct values versus the DNA concentration (Figure 1c). Average Ct values of the blood sample triplicates were placed on this standard curve (colored crosses) to determine the resulting DNA concentration (colored dashed lines). Figure 1d shows the plot of the resulting measured gDNA concentration versus the theoretically calculated gDNA concentration in the spiked blood sample based on dilution. The higher the input gDNA concentration, the higher is the measured gDNA concentration with a linear relationship for 2-fold serially

https://doi.org/10.1021/acssensors.2c02169
ACS Sens. 2023, 8, 673−683

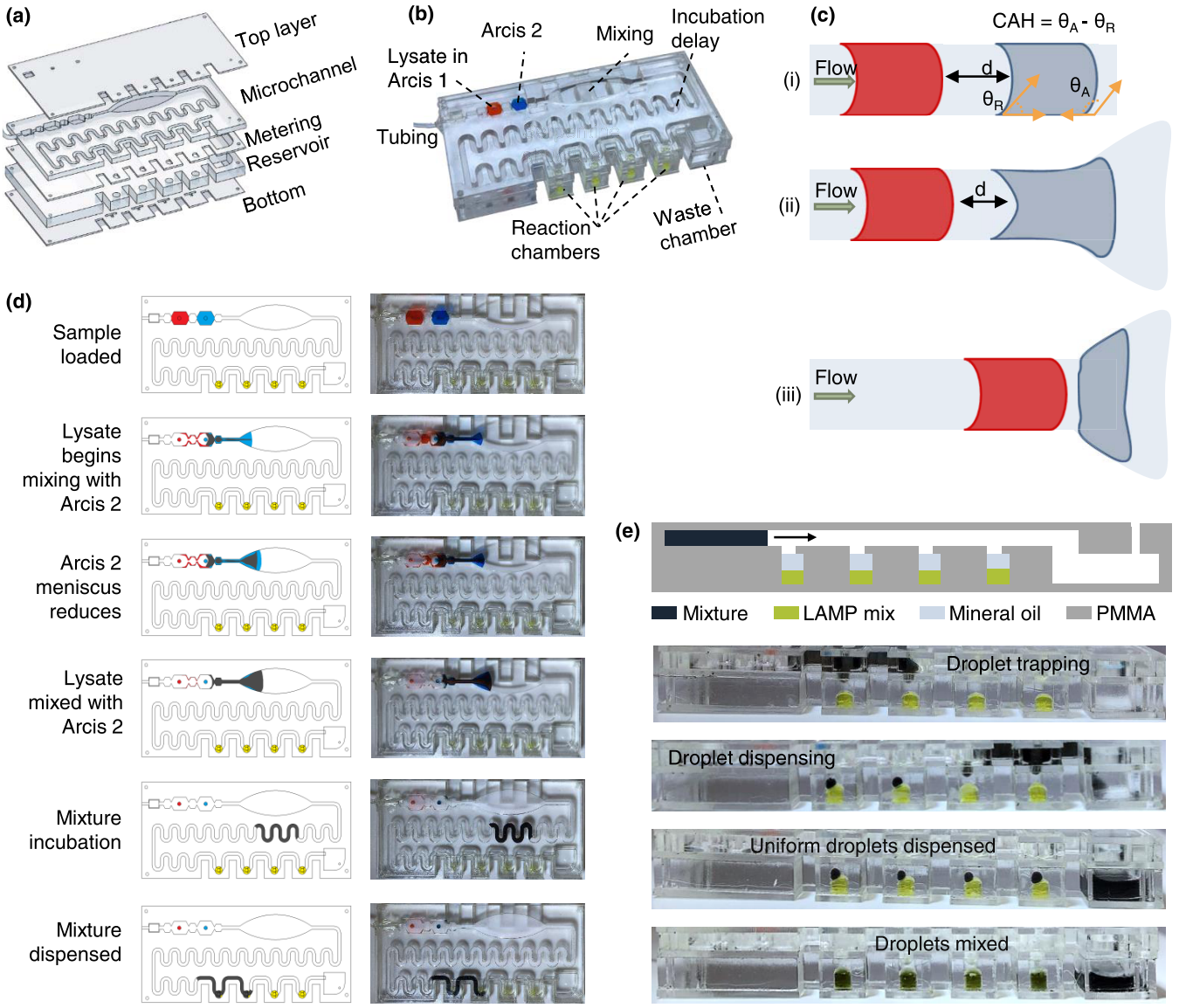

Figure 2. (a) Details of each layer of the PMMA cartridge: the top, metering, and bottom layers are 1 mm thick, the microchannel layer is 3.17 mm thick, and the reservoir layer is 5.65 mm thick. (b) Assembled cartridge along with details of each chamber. Chambers for lysate in Arcis 1 and Arcis 2 have a volume of 150 μL, reaction chambers have a volume of ~70 μL, and semicircular metering chambers have a volume of ~4 μL. (c) Use of elliptical structure to mix two sequentially loaded liquids. (d) Top view of the sample preparation process on the microfluidic cartridge. (e) Front view of the microfluidic cartridge showing various stages of the mixture dispensing step.

diluted gDNA as input (the highest concentration was 50 ng/μL). It must be noted that after the extraction procedure, blood samples spiked with 0.39 and 0.19 ng/μL diluted gDNA did not show any amplification within 55 cycles indicating dilution of the blood sample beyond the detection limits of the assay. This validates that the Arcis sample preparation protocol does not vary with gDNA concentration and preserves the gDNA quality for detection using downstream analysis.

To validate the LAMP assay, we performed real-time LAMP on the same samples used for qPCR. The LAMP curves are shown in Figure 1e, and the correlation between LAMP times to positive and qPCR cycle threshold values is shown in Figure 1f. A Pearson's coefficient of 0.94 suggests that the purification-free sample preparation is valid for both PCR and LAMP downstream analyses. These results confirmed the Arcis Sample Prep Kit as an acceptable sample preparation protocol with minimal background interference.

Continuous Flow Microfluidic Cartridge for the Automated Test. One of the significant challenges for NATs at the PON is related to the front end of the assays, NA extraction from raw samples.[37] The ideal sample preparation for malaria mass screening applications should be simple, scalable, and easy to operate. In this work, we have developed a disposable poly(methyl methacrylate) (PMMA) microfluidic cartridge to perform the previously described blood sample preparation and DNA amplification in a safe, hassle-free, and automated manner. The microfluidic cartridge consists of five PMMA layers and measures 10 cm × 4.5 cm × 1.2 cm (Figure 2a). Figure 2b is a picture of the assembled PMMA cartridge and highlights the various chambers using colored water. The top layer seals the cartridge and has inlet holes for each chamber, described further. The microchannel layer features two octagonal chambers (150 μL) for loading the blood lysate (red) and holding Arcis 2 (blue), an ellipsoid-shaped mixing

https://doi.org/10.1021/acssensors.2c02169
ACS Sens. 2023, 8, 673−683

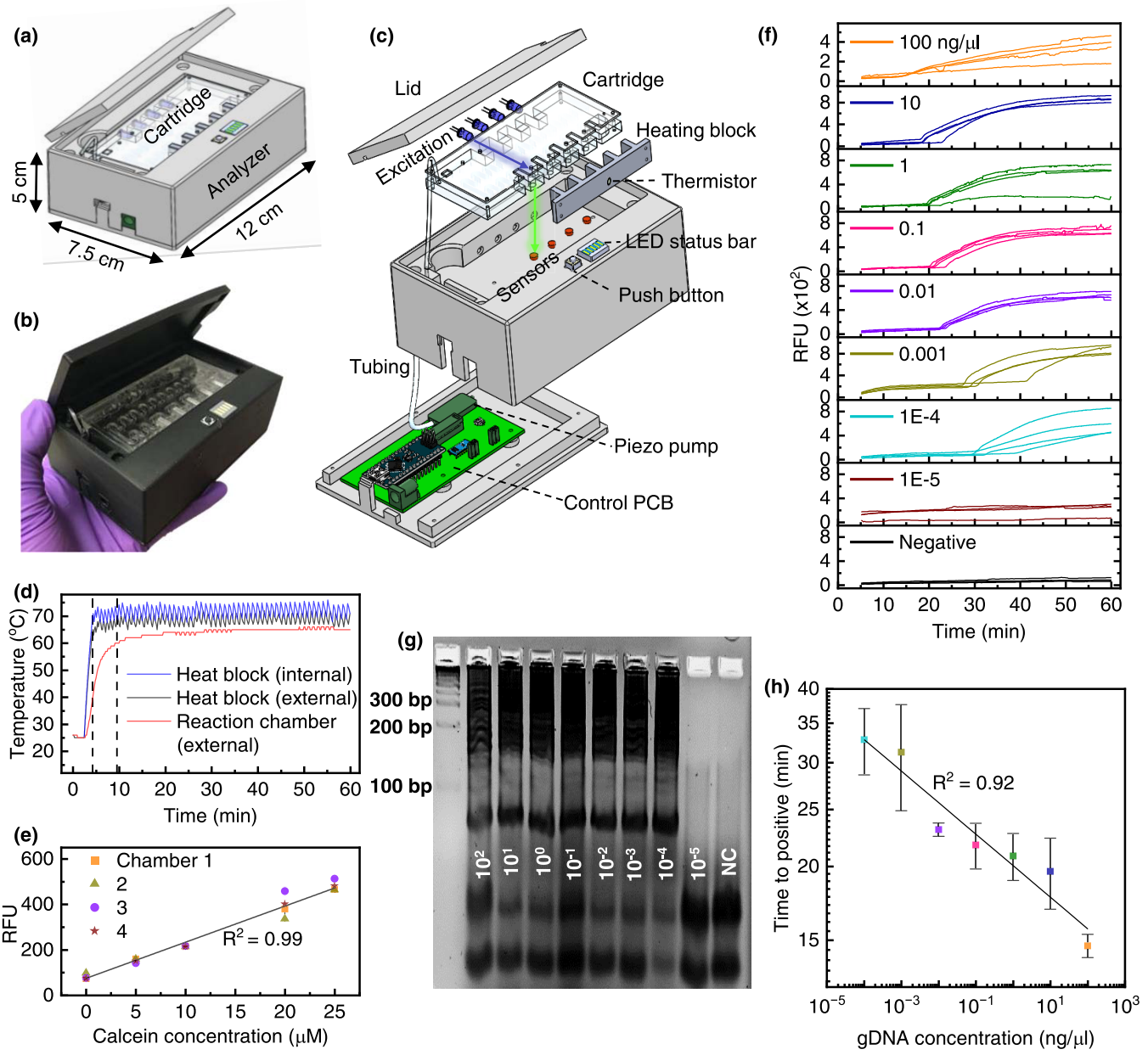

Figure 3. (a) Schematic of the instrument developed for streamlined, automated pressure-driven blood sample preparation for LAMP analysis on a microfluidic cartridge. (b) Image of the assembled instrument along with the PMMA microfluidic cartridge. (c) Detailed view of various modules of the instrument. (d) Heating kinetics were measured by pipetting 25 μL of H_2O and 45 μL of mineral oil into the microfluidic cartridge's LAMP reaction chambers. The heating block's temperature is regulated to 71 °C by the onboard Arduino Nano within 5 min. An external sensor was used to measure the temperature of the water by placing the thermistor inside the LAMP chamber. The LAMP chamber contents take another 5 min to reach ~62 °C and remain within the required LAMP temperature range at 64.61 ± 0.83 °C. (e) Color sensor characterization was performed by pipetting 25 μL fluorescence (calcein) of varying concentrations into all four chambers of the cartridge, and RFUs (red channel counts) were recorded for five min. A linear relationship with increasing concentration and consistency among all four chambers is seen. The error bars represent the variation of one channel over 5 min. (f) *Pf* gDNA amplification on the instrument. Ten-fold serially diluted *Pf* gDNA (10^2–10^{-5} ng/μL) and LAMP mix were manually pipetted into all four cartridge chambers and amplified. (g) Gel electrophoresis image of the amplicons confirms gDNA amplification on the instrument. The smear and banding pattern around the 200 bp rung confirm the LAMP amplification of *Pf* gDNA. As expected, the smear pattern is not seen for 10^{-5} ng/μL concentration and NC (water). The bands seen below the 100 bp rung are due to the LAMP primers. (h) Times to positive for each gDNA concentration. Error bars represent the standard deviation among the four chambers.

chamber, and a serpentine structure to induce an incubation delay. The metering layer features semicircular traps to isolate the mixture and generate a droplet of tunable volume that will combine with the LAMP master mix preloaded in the four reaction chambers (volume ~ 70 μL, yellow) in the reservoir layer. The undeposited mixture is drained into the waste chamber of the reservoir layer. The waste chamber also has an outlet to release the pressure exerted by the pump. To avoid the mixing of reagents during a fall or any other vibration, a passive check valve is employed by sandwiching an air-filled chamber between two teeth-shaped structures. Structural pinning is enabled by the tooth's sharp bending angle and radically increases the liquid–vapor interface area and raises the activation energy, thus preventing the fluid from overcoming

https://doi.org/10.1021/acssensors.2c02169
ACS Sens. 2023, 8, 673–683

the barrier. These passive valves are present on either side of the octagonal reagent chambers in the microchannel layer.

First, the blood sample is mixed with the Arcis 1 reagent off the cartridge in a microcentrifuge tube, and then, this lysate is loaded into the cartridge. All other necessary components, such as Arcis 2, LAMP mix, and mineral oil, are loaded in the cartridge before the test or could be preloaded (although not tested in the present study). A small piezo pump drives the lysate and Arcis 2 in the next chamber through the cartridge. A challenge in continuous flow microfluidics is mixing two sequentially loaded liquids due to laminar flow in the channel. However, they may mix in a sufficiently long channel while relying on diffusive mixing, an inherently slow process.[38] We exploit a hydrophilic surface's inherent contact angle hysteresis to speed up the mixing process. Contact angle hysteresis (CAH) is the difference between the advancing (θ_A) and receding (θ_R) angles,[39] which causes the droplet to elongate along the hydrophilic surface since the liquid is pinned at the receding point. In a uniform, straight channel, despite the contact angle hysteresis, the pressure builtup between the two liquid volumes is higher than the pinning force at the receding point, not allowing them to mix (Figure 2c(i)). As Arcis 2 approaches the ellipsoid-shaped structure, it prefers to flow closer to the edges and is pinned due to the hydrophilic nature of the laser-cut edge. Thus, its meniscus reduces, allowing the lysate mixture to compress the air and reduce the distance (d) it must travel to meet Arcis 2. The ellipsoid-shaped structure increases the contact area and contact time between the lysate and Arcis 2, beginning the mixing process. This mechanism is highlighted in Figure 2c(ii,iii). Figure 2d depicts the top views of the blood sample preparation instances. The serpentine structure also facilitates the mixing by generating chaotic advection,[40] thus improving the mixing efficiency.

Finally, the mixed fluid encounters the semicircular metering structure lined vertically above the LAMP chamber. It is used to dispense fixed amounts of the mixed fluid into the chamber by first isolating the fluid and then letting the 4 μL droplet sink through the mineral oil layer to combine with the LAMP master mix. The straight edge of the semicircular trap blocks any isolated fluid from being carried over to the next chamber. An equal amount of mixed fluid is isolated and dispensed by ensuring that the exact amount of mineral oil is loaded into each LAMP chamber. A surfactant added to the mineral oil assists the droplet in breaking the surface barrier between the mineral oil and the LAMP master mix. The cylindrical LAMP reaction chambers are loaded with 21 μL of LAMP mix and covered by 45 μL of mineral oil (with Span-80 as the surfactant). The metering trap process and droplet-dispensing instances are depicted in Figure 2e. The remaining volume of mixed fluid travels further and is deposited in subsequent LAMP reaction chambers, and the rest is flushed into the waste chamber. Although colored dyes were used to depict the process, the Supporting Video shows the top and front view of the sample preparation process with a blood sample, Arcis 2, and LAMP mix.

Instrument Design and Validation. Figure 3a,b depicts the developed instrument with a microfluidic cartridge. The palm-held instrument measures 12 (l) × 7.5 (w) × 5 cm (h). It is designed to perform automated blood sample preparation, followed by LAMP seamlessly on a microfluidic cartridge. A commercially available 23,000 mAh Li-ion battery pack powers the instrument for ∼65-min long tests. The instrument consists of a piezo pump to drive the reagents through the cartridge, an aluminum heating block to provide the heat required for the LAMP reaction, an optics assembly to monitor the fluorescence emitted from the reaction in real time, a press button to start the test, and a LED bar for user feedback. The real-time amplification values are recorded as RFU and stored on a computer which can be plotted later. However, the built-in LED bar provides intermediate updates during the test and displays the end point results, allowing the instrument's independent use. Figure 3c shows the disassembled view of the instrument, highlighting all of the comprising modules (described ahead), and Supporting Figure S1 shows a simplified block diagram. Supporting Figure S2 estimates that the instrument consumes 3.087 Wh over ∼65 min; this translates to 343 mAh at 9 V. Since the 23,000 mAh Li-ion battery pack uses cells with a nominal voltage of 3.7 V, some energy is lost in upconversion to 9 V (the operating voltage of the instrument). This leaves us with ∼7565 mAh at 9 V, enough to perform ∼20 tests on one charge.

Thermal Module. A custom fin-structured heating block is designed to heat the reaction contents to a LAMP conducive temperature. ∼1.08 A current at 9 V is driven across four 2-Ω power resistors (connected in series) attached to the aluminum heating block using a thermally conductive adhesive. A thermistor integrated into the heating block is used as internal feedback to regulate the desired temperature. As shown in Figure 3d, it takes ∼4 min for the aluminum heat block to reach ∼70 °C while the instrument sits in a room-temperature environment. The LAMP reaction chamber contents (25 μL of H_2O with 45 μL of mineral oil) take another 5 min to reach ∼62 °C and remain within the required LAMP temperature range after that, with a mean of 64.61 ± 0.83 °C. Although this characterization experiment was performed at room temperature, we opine that the instrument would need slightly more or less time in lower- or higher-temperature environments, respectively. However, this would not have a significant effect on the power consumption.

Optical Module. A blue (λ = 465 nm) excitation LED and a CMOS-based TCS 34725 color sensor pair is used as an optical readout to monitor the fluorescence emitted from a reaction chamber in real time. The excitation light from the LED is directed perpendicular to the optical sensor's field of view to minimize the excitation interference (refer to Figure 3c). Figure 3e shows a linear relationship between the concentration of fluorescent calcein (0−25 μM) loaded into the LAMP reaction chambers and the measured RFUs or photon counts. This validates the color sensors use to distinguish the real-time fluorescence increase of the LAMP reaction. Red counts from the sensor were used as RFU as they are least affected by the blue excitation light (data not shown). The error bars represent the variation of one channel over 5 min. Since the simplified optical assembly does not use any filters, some excitation light leaks into the color sensor while illuminating the reaction chamber; hence, it is essential to model the signal to differentiate the fluorescence from the background excitation. The signal (number of photons) captured by the color sensor is given by S_i, where i denotes the color sensor number (one through four).

$$S_i(t) = \frac{I_i \beta_i}{h\nu}[\alpha C_i(t)\phi_F + N_{Bi}\phi_B] \times T_i \quad (1)$$

where I_i is the LED's output power, β_i is the coupling factor between a reaction chamber's emission and the sensor, $h\nu$ is the emitted photon's energy, α is the absorption coefficient, C_i is the fluorescence concentration that is unquenched as the LAMP reaction proceeds, ϕ_F is the fluorescence quantum yield, N_{Bi} is the background signal (not dependent on the fluorescence

https://doi.org/10.1021/acssensors.2c02169
ACS Sens. 2023, 8, 673−683

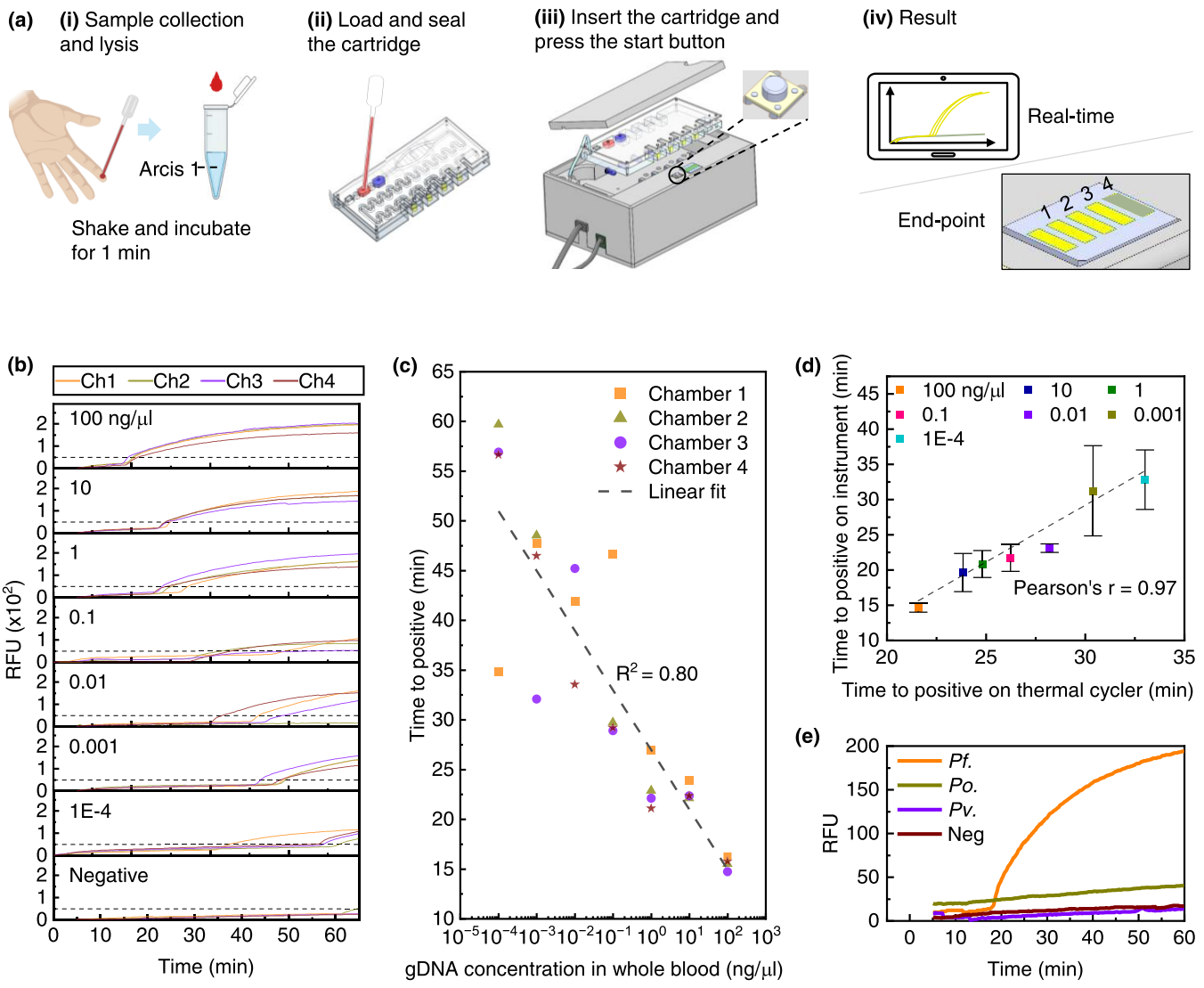

Figure 4. (a) Proposed test workflow: (i) collect 40 μL of the blood sample into a tube containing 120 μL of Arcis 1 reagent, shake well, and incubate for 1 min. (ii) Transfer 150 μL of the blood lysate (denoted by red) to the microfluidic cartridge that is preloaded with Arcis reagent 2 (denoted by blue) and LAMP master mix (denoted by yellowish green) topped with mineral oil. (iii) Connect the microfluidic cartridge's tubing to the piezo pump, place it in the recess, and close the lid. Once the start button is pressed, autonomous sample preparation begins by mixing the lysate and Arcis reagent 2 and dispensing the mixture into the four LAMP reaction chambers, followed by LAMP for 60 min. (iv) Real-time LAMP results can be plotted on a computer screen, or end point results can be displayed on the status LED bar. The numbers one through four represent the LAMP chambers. (b) Amplification curves for contrived blood samples prepared by spiking 36 μL of whole blood with 4 μL of 10-fold serially diluted *Pf* gDNA (10^2–10^{-4} ng/μL). Lysis with Arcis 1 was performed in a tube, followed by further autonomous processing of the resulting mixture in the cartridge on the analyzer. A quick evaluation warrants setting the threshold at 50 RFU. (c) Time to positive vs gDNA concentration in contrived blood samples. Parasite concentration was determined using the relation one parasite = 2.35×10^{-5} ng. A quick investigation suggests a sensitivity of 0.42 parasites/μL. (d) Pearson correlation between time to positive seen on the instrument using automated sample preparation and detection on the cartridge and benchtop thermal cycler using manual sample preparation steps (same as Figure 1e). (e) Analytical specificity test using other *Plasmodium* gDNA spiked in whole blood. Contrived blood samples were processed with Arcis 1 and Arcis 2 in tubes, and LAMP was performed on the cartridge in the instrument simultaneously. Only the *Pf* gDNA-spiked blood sample (10^2 ng/μL) was amplified, while the *Pv* and *Po* gDNA-spiked blood samples, and the nonspiked blood remained negative.

concentration and contributed by the leaked excitation), ϕ_B is the background signal quantum yield, and T_i is the integration time (a changeable parameter of the sensor). For simplicity, we consider T_i is multiplied instead of convolved with the other parameters. The excitation light coupled to each reaction chamber may not be the same due to the chamber's distance from the LED and the overall arrangement. Moreover, the fluorescence coupled to each color sensor may not be the same, resulting in nonuniformity among the reaction chambers.

At $t = 0$, the fluorescence concentration $C_i = 0$. Thus, the signal is given as

$$S_i(0) = \frac{I_i \beta_i}{h\nu}[N_{Bi}\phi_B] \times T_i \tag{2}$$

To make chamber 2's signal similar to chamber 1, each reading must be divided by a scaling factor (SF) which is given by the ratio of $S_2(t = 0)$ *and* $S_1(t = 0)$. Subsequently, the background signal must be subtracted, $S_2(t) - S_2(0)$. Thus, every new signal is given as

https://doi.org/10.1021/acssensors.2c02169
ACS Sens. 2023, 8, 673−683

$$\widehat{S}_i(t) = \frac{S_i(t)}{SF_i} - \frac{S_i(0)}{SF_i} \quad (3)$$

Thus, at $t = 0$, all chamber sensors must not have any signal due to fluorescence, and the background/baseline must be subtracted from the color sensor reading to represent true amplification RFUs. This is accommodated in two stages, explained further in the Methods section.

Pneumatic Module. The Arcis sample preparation protocol is implemented on the microfluidic cartridge using a piezo pump from Bartels Mikrotechnik, Germany. It is a miniaturized double diaphragm pump with passive check valves, measuring 30 mm × 15 mm × 3.8 mm and weighing 2 g. The piezo pump is interfaced with a microcontroller (MCU) via a driver circuit also manufactured by Bartels Mikrotechnik. The driver circuit allows us to control the pump's flow rate in real time between 0 and 7 mL/min by adjusting the operating voltage and frequency. Such use of the piezo pump avoids the need for any rotational element/moving part, like in centrifugal-force-based platforms that may need large amounts of electrical power to achieve high rotational speeds for the desired nonlinear centrifugal forces. The pump is connected to the microfluidic cartridge by a Tygon tube.

Instrument Validation. To evaluate the quantitative testing ability of this diagnostic platform, we subjected a series of 10-fold dilutions of purified *Pf* gDNA in Tris-EDTA buffer to LAMP reactions in the instrument. For each concentration, a set of four identical reactions were prepared by manually pipetting 24 μL of LAMP master mix and a 1 μL gDNA sample into each of the four reaction chambers on the cartridge. Figure 3f shows real-time amplification curves (one replicate in each reaction chamber of the cartridge) of tests carried out for each concentration and water as a negative control (NC). 10^{-5} ng/μL and NC (water) were not amplified within 65 min. A trend of delayed pick-up times for decreasing concentration is seen in these amplification curves and the variation in times to positive increases for concentrations below 0.01 ng/μL. At low gDNA concentrations (0.001 and 1×10^{-4} ng/μL), the amplification curves have slight dissimilarity, possibly due to any LAMP assay's highly efficient but semiquantitative amplification mechanism. The amplified products of each starting concentration were extracted from the cartridge and subjected to gel electrophoresis (5% agarose gel), and the image is shown in Figure 3g. The smear and banding pattern around the 200 bp rung confirms the LAMP amplification of *Pf* gDNA. As expected, the smear pattern is not seen for 10^{-5} ng/μL concentration and NC (water). The bands seen below the 100 bp rung are due to the LAMP primers (F3, B3, LB, and LB: ∼20 bp, BIP: 40 bp, and FIP: 50 bp). Figure 3h shows the mean times to positive for each concentration along with the standard deviation. A clear linear relationship ($R^2 = 0.92$) is observed between time to positive and the *Pf* gDNA concentration between 10^2 and 10^{-4} ng/μL, which could be used as a reference curve for quantification.

Detection of *Pf* gDNA in Contrived Whole Blood Samples. Figure 4a describes the proposed workflow of the blood sample to answer molecular diagnostic test: (i) a 40 μL finger-prick blood sample is added into a microcentrifuge tube containing 120 μL of Arcis 1 reagent, shaken, and incubated at room temperature for 1 min. Arcis 1 works as a lysis agent to release DNA in the blood. It simultaneously chelates the other NAs and stabilizes the DNA. (ii) The first octagonal chamber of the microfluidic cartridge is loaded with 150 μL of this lysate, and the inlet hole is sealed (shown by red dye). (iii) The cartridge is then placed into the instrument, and a Tygon tube attached to the cartridge is connected to the piezo pump. Upon pressing the button, the instrument begins the test by preparing the sample by mixing the blood lysate with Arcis 2 (piezo pump driven), which removes the NA chelation and relaxes the DNA while binding any LAMP inhibitors present in the blood that may prevent amplification of the DNA. Mixing is seamlessly followed by automated dispensing of the sample into LAMP reaction chambers preloaded with the LAMP master mix. The heating block surrounding the LAMP reaction chamber from three sides heats up the mixture inside to ∼64 °C to start the amplification reaction, which is monitored in real time using the color sensors. The sample preparation takes about 3 min, followed by the amplification process, which takes up to 60 min. (iv) The real-time amplification can be plotted on a connected computer, and the final test result (positive or negative) can be displayed on the built-in status LED bar. A test is reported positive if the majority of reaction chambers (three of the four) show amplification of the *Pf* gDNA in the blood sample, allowing us to be confident of the positive/negative call.

To evaluate our instrument's performance for a whole blood sample in a laboratory, we used mock blood samples spiked with extracted gDNA. Briefly, we spiked 36 μL of whole blood with 4 μL of 10-fold serially diluted *Pf* gDNA (10^2–10^{-4} ng/μL) to create mock samples. After lysing the blood sample with Arcis 1 in a tube, the resulting mixture was processed on a microfluidic cartridge and subjected to LAMP on the instrument. Figure 4b shows amplification curves for each spiked whole blood sample. Since 10^{-5} ng/μL purified *Pf* gDNA was not amplified, we did not attempt amplifying any 10^{-5} ng/μL spiked blood samples. Although estimation of the limit of detection requires the times to positive be expressed as a probability with confidence intervals, we use the relation, one parasite = 23×10^6 bp = 0.0235 pg gDNA,[41] to suggest the whole blood sensitivity. 4×10^{-4} ng/μL gDNA in 40 μL of blood corresponding to 10^{-5} ng/μL of whole blood is reproducibly detected on the instrument. Thus, we estimate the sensitivity as 0.42 parasite/μL. This is agreeable with WHO's analytical sensitivity estimate to be lower than two parasites/μL for identifying low-level infection in a pre-elimination setting. One may notice that for 0.01 ng/μL, only three out of the four reaction chambers showed amplification; this could be due to the low amount of sample dispensed into that particular reaction chamber. Additionally, the variation in times to positive increases for concentrations below 0.1 ng/μL, which could be attributed to the semiquantitative ability of any LAMP assay compared to a PCR assay.[42] Figure 4c shows the linear ($R^2 = 0.80$) and inversely proportional relationship between the time to positive and parasite concentration. As expected, the standard deviation between the time to positive increases as the parasite concentration decreases. However, the strong linear relationship can be exploited to quantify parasitemia in whole blood samples.

To further benchmark our instrument with a benchtop thermal cycler, we used mock blood samples spiked with 10^2–10^{-4} ng/μL gDNA (10x serially diluted) that were subject to Arcis reagent-based sample preparation in traditional microcentrifuge tubes for LAMP analysis on a benchtop thermal cycler (triplicates). This process is the same as that described in Figure 1e. Figure 4d shows the correlation between times to positive seen on the instrument using automated sample preparation along with detection on the cartridge and benchtop thermal cycler using manual sample preparation steps. A Pearson's $R = 0.97$ indicates a good agreement between the automated

https://doi.org/10.1021/acssensors.2c02169
ACS Sens. 2023, 8, 673−683

instrument and manual setup. The amplification curves and times to positive of the LAMP reactions performed on the benchtop thermal cycler are given in Supporting Figure S3.

To confirm the analytical specificity of the test, we prepared four separate whole blood samples, three spiked with *Pf*, *Pv*, and *Po* gDNA, as explained earlier, and a nonspiked one. Since the microfluidic cartridge is designed to dispense the same blood sample into the four reaction chambers, the Arcis sample preparation protocol was carried out in tubes, as explained earlier. The four products and the LAMP master mix were manually pipetted into the four cartridge chambers to simultaneously run an amplification experiment on all samples. As seen in Figure 4e, only the *Pf* gDNA-spiked blood sample was amplified, while the *Pv* and *Po* gDNA-spiked blood samples and the nonspiked blood sample remained negative for 65 min.

The readers should note that the LAMP assay used to test the instrument's performance for a whole blood sample has been previously evaluated for thermostability.[25] Briefly, enzymes and reagents retained sufficient activity to achieve successful DNA amplification when stored at 4 °C for a week, and there was no significant shift in the average threshold time. However, when stored at 25 °C, the enzymes and reagents were active for three days (no activity afterward), and the threshold time needed to obtain the positive/negative results was delayed. Although not evaluated, the PMMA cartridge used in the current study could interact with the reagents differently when compared to Eppendorf tubes used to test the thermostability in the previous study. Being aware of the critical need for field deployable PON NATs, we are diligently working to develop a protocol for lyophilized LAMP assay, a more user-friendly and transport-friendly industry standard. We aim to lyophilize the regents directly in a cartridge and then test the long-term stability and shelf-life over a seven-week interval. When tested with a relevant cartridge design, these results will be published in a future study.

Another point to be noted is that the first step of sample preparation (lysis) is also performed off-chip in a micro-centrifuge tube containing Arcis 1. It has been designed to be analogous to the step of blood sample collection in a tube containing an anticoagulant (for example, EDTA). Thus, it does not add any significant complexity to the proposed test workflow despite the manual lysis step.

CONCLUSIONS

A handheld malaria testing device capable of running four parallel reactions was developed and validated using contrived whole blood samples. The automated reagent-based sample preparation and the real-time LAMP reaction have been seamlessly integrated into a single-use continuous flow microfluidic cartridge. Although the microfluidic cartridge is configured to run four identical reactions, it can be scaled up and modified to run a blood sample while comparing with internal controls (high parasitemia, medium parasitemia, and negative sample). This, along with a quantitative ability, will enable the estimation of parasite load in an infected blood sample. We report an analytical sensitivity of ∼0.42 parasite/μL, apt to identify asymptomatic infected carriers. Alternatively, the microfluidic cartridge could be configured to run species-specific LAMP assays in the four reaction chambers to identify whether the sample is infected with *Pf*, *Pv*, *Po*, or *Pm*, similar to our previous work.[25] This portable, low-cost, sensitive, specific, and real-time LAMP PON test would prove to be very useful in remote and resource-limited settings for screening purposes toward malaria elimination. Some modification to the microfluidic cartridge seems necessary to make the test truly fit for PON applications. The lysis process of combining whole blood with Arcis 1 could be moved to the cartridge for "sample-in," "answer-out" analysis. Although our platform promises more sensitive screening than antigen tests, rigorous testing with clinical samples is needed before on-field deployment.

METHODS

Instrument Design and Fabrication. The instrument comprises 3D printed structural parts, a machined aluminum heating block, a piezo pump, electronics such as Arduino Nano (MCU), excitation LEDs, and color sensors for fluorescence detection. Three-dimensional printed structural parts and the machined aluminum heating block were designed in Solidworks CAD software. Three-dimensional printed structural parts were fabricated using MakerBot Method X 3D printer (Brooklyn, NY) with MakerBot ABS (acrylonitrile butadiene styrene) material. The thermal module uses four 2-Ω power resistors (MP725-2.00) mounted on the aluminum heating block using a thermally conductive adhesive paste (Arctic Alumina) and an MC65F103A 10 k-ohm thermistor (Amphenol Thermometrics, St. Mary's, PA) mounted in a small recess in the heating block. PCBs were designed in AutoDesk Eagle CAD software and fabricated by OSH Park LLC (Lake Oswego, OR). The optical module PCB consists of four blue excitation LEDs (04R6674, Cree LED) purchased from Adafruit Industries (New York, NY) and four color sensors (TCS 34725, AMS AG, Premstaetten, Austria) purchased from DigiKey.com. The main body houses the thermal, optical, and pumping modules, while the motherboard PCB is mounted on the bottom of the enclosure.

Microfluidic Cartridge Fabrication. The microfluidic cartridge consists of five PMMA layers of varying thicknesses and is designed in AutoDesk AutoCAD software. The top, metering, and bottom layers are 1 mm thick, the microchannel layer is 3.17 mm thick, and the reservoir layer is 5.65 mm thick. A pressure-sensitive adhesive (PSA) tape from Flexcon was applied to each PMMA sheet, and then, structures were patterned using a VLS3.60DT CO_2 Laser cutter (Universal Laser Systems, Scottsdale, AZ). All layers are aligned by inserting dowel pins into alignment holes designed on all four corners of the PMMA layers and assembled by pressing them together.

Human Whole Blood. Single donor human whole blood with K2 EDTA anticoagulant (Lot#: HMN696957) was purchased from Innovative Research. It was collected at an FDA-approved collection center, tested for standard FDA-required viral markers, and found negative for HBsAg, HCV, HIV-1, HIV-2, HIV-1Ag or HIV-1 NAT, ALT, West Nile virus NAT, Zika NAT, and syphilis using FDA-approved methods by the vendor.

qPCR Assay. As shown in Supporting Tables S1 and S2, we used PrimeTime Gene Expression Master Mix (1X), 0.3 μM forward and reverse primers along with a 0.2 μM probe with Express PrimeTime 5′ HEX as a reporter and /ZEN/3′ IBFQ as a dual quencher, and 1 μL of sample in a 25 μL reaction. The primer and probe design was adapted from ref43 and manufactured by IDT, Coralville, USA. The reaction steps included heating at 95 °C for 3 min to activate the polymerase, followed by 55 cycles of heating to 95 °C for 15 s and cooling down to 60 °C for 1 min, as per the PCR master mix's manufacturer (Supporting Table S3). To mimic an infected blood sample, 9 μL of negative whole blood was spiked with 1 μL of *Pf* gDNA (3D7 stage, stock concentration 50 ng/μL). Nine such blood samples were prepared by serially diluting the gDNA 2-fold. Each blood sample was subjected to DNA extraction by incubating it with 30 μL of Arcis reagent 1 for 1 min and then mixing 20 μL of the resulting lysate with 20 μL of Arcis reagent 2. A nonspiked blood sample was also prepared in the same manner. One microliter of this mixture was used in the final PCR amplification analysis. Triplicates of each blood sample and serially diluted purified gDNA were subjected to PCR on the same 96-well plate in a BioRad CFX96 benchtop thermal cycler.

LAMP Assay. Refer to Supporting Tables S4 and S5 for the LAMP reaction mix, which consists of isothermal buffer (20 mM Tris-HCl, 10 mM $(NH_4)_2SO_4$, 50 mM KCl, 2 mM $MgSO_4$, 0.1% Tween 20, pH 8.8), *Pf*-specific primer set (5 pmol F3 and B3, 40 pmol FIP and BIP, 20 pmol

https://doi.org/10.1021/acssensors.2c02169
ACS Sens. 2023, 8, 673−683

LF and LB) manufactured by IDT, $MgSO_4$, calcein, $MnCl_2$, deoxyribonucleotide triphosphates (dNTPs), *Bst* 2.0 DNA polymerase, DNA template, and PCR grade H_2O. The LAMP assay was performed at a constant temperature of ∼64 °C. The primer set was first reported by[44] and used in our previous studies.[25,45]

Data Processing to Generate Uniform Curves and Identify the Time to Positive. As explained in the Results and Discussion section, raw data collected from the color sensors must be processed to generate uniform amplification curves since excitation signals may be inherently different. The raw data as collected is shown in Supporting Figure S4a. Step 1 is scaling the amplification signals of the second, third, and fourth chambers to the first chamber signal as reference (Supporting Figure S4b). It must be noted that the values collected over the first 5 min have been ignored since the temperature of the LAMP reaction chamber contents is rising over this period. Step 2 is subtracting the background signal acquired within the first 5 min from every subsequent value (Supporting Figure S4c). This approach is similar to our previous work.[46] Although a receiver operating characteristic (ROC) curve must be plotted to statistically determine a threshold to classify an amplification curve as positive or negative, a quick evaluation warrants setting a threshold of 50 RFU for testing blood samples. The times to positive are obtained when the amplification curves intersect/cross the 50 RFU threshold line.

■ ASSOCIATED CONTENT

Supporting Information

The Supporting Information is available free of charge at https://pubs.acs.org/doi/10.1021/acssensors.2c02169.

Figures showing instrument system, an estimation of the power consumption per test, and the methodology used for data processing and multiple tables detailing the LAMP and PCR primer sets, the recipe for LAMP and PCR master mixes, and the bill of materials for the instrument development (PDF)

Supporting Video depicting the pressure-driven microfluidic sample preparation of a whole blood sample is also submitted (MP4)

■ AUTHOR INFORMATION

Corresponding Author

Weihua Guan − *School of Electrical Engineering and Computer Science, Pennsylvania State University, University Park, Pennsylvania 16802, United States; Department of Biomedical Engineering, Pennsylvania State University, University Park, Pennsylvania 16802, United States;* orcid.org/0000-0002-8435-9672; Email: wzg111@psu.edu

Authors

Aneesh Kshirsagar − *School of Electrical Engineering and Computer Science, Pennsylvania State University, University Park, Pennsylvania 16802, United States;* orcid.org/0000-0003-2288-5439

Gihoon Choi − *School of Electrical Engineering and Computer Science, Pennsylvania State University, University Park, Pennsylvania 16802, United States;* Present Address: G.C.: Sandia National Laboratories, Biotechnology & Bioengineering Dept., Livermore, California 94550, United States

Vishaka Santosh − *U.S. Army, DEVCOM Chemical Biological Center, Aberdeen Proving Ground, Maryland 21010, United States*

Tara Harvey − *U.S. Army, DEVCOM Chemical Biological Center, Aberdeen Proving Ground, Maryland 21010, United States*

Robert Cory Bernhards − *U.S. Army, DEVCOM Chemical Biological Center, Aberdeen Proving Ground, Maryland 21010, United States*

Complete contact information is available at: https://pubs.acs.org/10.1021/acssensors.2c02169

Notes

The authors declare no competing financial interest.

The authors declare that they have no known competing financial interests or personal relationships that could have appeared to influence the work reported in this paper.

■ ACKNOWLEDGMENTS

This work was partially supported by the Defense Threat Reduction Agency (CWMD 1907), the National Science Foundation (1902503, 1912410), and the National Institutes of Health (R61AI147419). Any opinions, findings, conclusions, or recommendations expressed in this work are those of the authors and do not necessarily reflect the views of the DTRA, National Science Foundation, and National Institutes of Health.

■ REFERENCES

(1) World Health Organization. *World Malaria Report 2020: 20 Years of Global Progress and Challenges*; World Health Organization2020.

(2) Crompton, P. D.; Pierce, S. K.; Miller, L. H. Advances and challenges in malaria vaccine development. *J. Clin. Invest.* **2010**, *120*, 4168−4178.

(3) Edwin, G. T.; Korsik, M.; Todd, M. H. The past, present and future of anti-malarial medicines. *Malar. J.* **2019**, *18*, 1−21.

(4) Wu, L.; van den Hoogen, L. L.; Slater, H.; Walker, P. G. T.; Ghani, A. C.; Drakeley, C. J.; Okell, L. C. Comparison of diagnostics for the detection of asymptomatic *Plasmodium falciparum* infections to inform control and elimination strategies. *Nature* **2015**, *528*, S86−S93.

(5) Galatas, B.; Mayor, A.; Gupta, H.; Balanza, N.; Jang, I. K.; Nhamussua, L.; Simone, W.; Cisteró, P.; Chidimatembue, A.; Munguambe, H.; et al. Field performance of ultrasensitive and conventional malaria rapid diagnostic tests in southern Mozambique. *Malar. J.* **2020**, *19*, 1−15.

(6) Zephyr Biomedicals. FalciVax - Rapid test for Malaria. www.tulipgroup.com/Zephyr_New/html/product_specs/1_falcivax_B.htm (accessed April 20, 2022).

(7) Swarthout, T. D.; Counihan, H.; Senga, R. K. K.; Van den Broek, I. Paracheck-Pf accuracy and recently treated *Plasmodium falciparum* infections: is there a risk of over-diagnosis? *Malar. J.* **2007**, *6*, 1−6.

(8) Lee, J.-H.; Jang, J. W.; Cho, C. H.; Kim, J. Y.; Han, E. T.; Yun, S. G.; Lim, C. S.; Loeffelholz, M. J. False-Positive Results for Rapid Diagnostic Tests for Malaria in Patients with Rheumatoid Factor. *J. Clin. Microbiol.* **2014**, *52*, 3784−3787.

(9) Gatton, M. L.; Chaudhry, A.; Glenn, J.; Wilson, S.; Ah, Y.; Kong, A.; Ord, R. L.; Rees-Channer, R. R.; Chiodini, P.; Incardona, S.; et al. Impact of *Plasmodium falciparum* gene deletions on malaria rapid diagnostic test performance. *Malar. J.* **2020**, *19*, No. 392.

(10) Feleke, S. M.; Reichert, E. N.; Mohammed, H.; Brhane, B. G.; Mekete, K.; Mamo, H.; Petros, B.; Solomon, H.; Abate, E.; Hennelly, C.; et al. *Plasmodium falciparum* is evolving to escape malaria rapid diagnostic tests in Ethiopia. *Nat. Microbiol.* **2021**, *6*, 1289−1299.

(11) Joanny, F.; Löhr, S. J.; Engleitner, T.; Lell, B.; Mordmüller, B. Limit of blank and limit of detection of *Plasmodium falciparum* thick blood smear microscopy in a routine setting in Central Africa. *Malar. J.* **2014**, *13*, No. 234.

(12) Centers for Disease Control and Prevention. *Malaria Diagnostic Tests*, 2020. https://www.cdc.gov/malaria/diagnosis_treatment/diagnostic_tools.html#tabs-1-1 (accessed November 18, 2022).

(13) Berzosa, P.; de Lucio, A.; Romay-Barja, M.; Herrador, Z.; González, V.; García, L.; Fernández-Martínez, A.; Santana-Morales, M.; Ncogo, P.; Valladares, B.; et al. Comparison of three diagnostic

methods (microscopy, RDT, and PCR) for the detection of malaria parasites in representative samples from Equatorial Guinea. *Malar. J.* **2018**, *17*, No. 333.
(14) Ugah, U. I.; Alo, M. N.; Owolabi, J. O.; Okata-Nwali, O. D.; Ekejindu, I. M.; Ibeh, N.; Elom, M. O. Evaluation of the utility value of three diagnostic methods in the detection of malaria parasites in endemic area. *Malar. J.* **2017**, *16*, No. 189.
(15) Cordray, M. S.; Richards-Kortum, R. R. Emerging nucleic acid-based tests for point-of-care detection of malaria. *Am. J. Trop. Med. Hyg.* **2012**, *87*, 223−230.
(16) Snounou, G.; Viriyakosol, S.; Jarra, W.; Thaithong, S.; Brown, K. N. Identification of the four human malaria parasite species in field samples by the polymerase chain reaction and detection of a high prevalence of mixed infections. *Mol. Biochem. Parasitol.* **1993**, *58*, 283−292.
(17) Snounou, G.; Viriyakosol, S.; Xin Ping, Z.; Jarra, W.; Pinheiro, L.; do Rosario, V. E.; Thaithong, S.; Brown, K. N. High sensitivity of detection of human malaria parasites by the use of nested polymerase chain reaction. *Mol. Biochem. Parasitol.* **1993**, *61*, 315−320.
(18) Rougemont, M.; Saanen, M. V.; Sahli, R.; Hinrikson, H. P.; Bille, J.; Jaton, K. Detection of Four *Plasmodium* Species in Blood from Humans by 18S rRNA Gene Subunit-Based and Species-Specific Real-Time PCR Assays. *J. Clin. Microbiol.* **2004**, *42*, 5636−5643.
(19) Lucchi, N. W.; Demas, A.; Narayanan, J.; Sumari, D.; Kabanywanyi, A.; Kachur, S. P.; Barnwell, J. W.; Udhayakumar, V. Real-time fluorescence loop mediated isothermal amplification for the diagnosis of malaria. *PLoS One* **2010**, *5*, No. e13733.
(20) Surabattula, R.; Vejandla, M. P.; Mallepaddi, P. C.; Faulstich, K.; Polavarapu, R. Simple, rapid, inexpensive platform for the diagnosis of malaria by loop mediated isothermal amplification (LAMP). *Exp. Parasitol.* **2013**, *134*, 333−340.
(21) Hopkins, H.; González, I. J.; Polley, S. D.; Angutoko, P.; Ategeka, J.; Asiimwe, C.; Agaba, B.; Kyabayinze, D. J.; Sutherland, C. J.; Perkins, M. D.; Bell, D. Highly Sensitive Detection of Malaria Parasitemia in a Malaria-Endemic Setting: Performance of a New Loop-Mediated Isothermal Amplification Kit in a Remote Clinic in Uganda. *J. Infect. Dis.* **2013**, *208*, 645−652.
(22) Mohon, A. N.; Lee, L. D.-Y.; Bayih, A. G.; Folefoc, A.; Guelig, D.; Burton, R. A.; LaBarre, P.; Chan, W.; Meatherall, B.; Pillai, D. R. NINA-LAMP compared to microscopy, RDT, and nested PCR for the detection of imported malaria. *Diagn. Microbiol. Infect. Dis.* **2016**, *85*, 149−153.
(23) Lucchi, N. W.; Gaye, M.; Diallo, M. A.; Goldman, I. F.; Ljolje, D.; Deme, A. B.; Badiane, A.; Ndiaye, Y. D.; Barnwell, J. W.; Udhayakumar, V.; Ndiaye, D. Evaluation of the illumigene malaria LAMP: a robust molecular diagnostic tool for malaria parasites. *Sci. Rep.* **2016**, *6*, No. 36808.
(24) Rypien, C.; Chow, B.; Chan, W. W.; Church, D. L.; Pillai, D. R.; Gilligan, P. Detection of *Plasmodium* Infection by the illumigene Malaria Assay Compared to Reference Microscopy and Real-Time PCR. *J. Clin. Microbiol.* **2017**, *55*, 3037−3045.
(25) Choi, G.; Prince, T.; Miao, J.; Cui, L.; Guan, W. Sample-to-answer palm-sized nucleic acid testing device towards low-cost malaria mass screening. *Biosens. Bioelectron.* **2018**, *115*, 83−90.
(26) Xu, G.; Nolder, D.; Reboud, J.; Oguike, M. C.; van Schalkwyk, D. A.; Sutherland, C. J.; Cooper, J. M. Paper-Origami-Based Multiplexed Malaria Diagnostics from Whole Blood. *Angew. Chem., Int. Ed.* **2016**, *55*, 15250−15253.
(27) Chiu, D. T.; deMello, A. J.; Di Carlo, D.; Doyle, P. S.; Hansen, C.; Maceiczyk, R. M.; Wootton, R. C. R. Small but Perfectly Formed? Successes, Challenges, and Opportunities for Microfluidics in the Chemical and Biological Sciences. *Chem* **2017**, *2*, 201−223.
(28) Liu, T.; Choi, G.; Tang, Z.; Kshirsagar, A.; Politza, A. J.; Guan, W. Fingerpick Blood-Based Nucleic Acid Testing on A USB Interfaced Device towards HIV self-testing. *Biosens. Bioelectron.* **2022**, *209*, No. 114255.
(29) Shi, R.; Lewis, R. S.; Panthee, D. R. Filter paper-based spin column method for cost-efficient DNA or RNA purification. *PLoS One* **2018**, *13*, No. e0203011.
(30) Poh, J.-J.; Gan; Samuel, K.-E. Comparison of customized spin-column and salt-precipitation finger-prick blood DNA extraction. *Biosci. Rep.* **2014**, *34*, No. e00145.
(31) Vincent, J. P.; Komaki-Yasuda, K.; Iwagami, M.; Kawai, S.; Kano, S. Combination of PURE-DNA extraction and LAMP-DNA amplification methods for accurate malaria diagnosis on dried blood spots. *Malar. J.* **2018**, *17*, No. 373.
(32) Mens, P. F.; de Bes, H. M.; Sondo, P.; Laochan, N.; Keereecharoen, L.; van Amerongen, A.; Flint, J.; Sak, J. R. S.; Proux, S.; Tinto, H.; Schallig, H. D. F. H. Direct Blood PCR in Combination with Nucleic Acid Lateral Flow Immunoassay for Detection of *Plasmodium* Species in Settings Where Malaria Is Endemic. *J. Clin. Microbiol.* **2012**, *50*, 3520−3525.
(33) Sidstedt, M.; Hedman, J.; Romsos, E. L.; Waitara, L.; Wadsö, L.; Steffen, C. R.; Vallone, P. M.; Rådström, P. Inhibition mechanisms of hemoglobin, immunoglobulin G, and whole blood in digital and real-time PCR. *Anal. Bioanal. Chem.* **2018**, *410*, 2569−2583.
(34) Shin, J. H.Nucleic Acid Extraction and Enrichment. In *Advanced Techniques in Diagnostic Microbiology: Volume 1: Techniques*; Tang, Y.-W.; Stratton, C. W., Eds.; Springer International Publishing, 2018; pp 273−292.
(35) Yin, J.; Suo, Y.; Zou, Z.; Sun, J.; Zhang, S.; Wang, B.; Xu, Y.; Darland, D.; Zhao, J. X.; Mu, Y. Integrated microfluidic systems with sample preparation and nucleic acid amplification. *Lab Chip* **2019**, *19*, 2769−2785.
(36) Schrader, C.; Schielke, A.; Ellerbroek, L.; Johne, R. PCR inhibitors − occurrence, properties and removal. *J. Appl. Microbiol.* **2012**, *113*, 1014−1026.
(37) Dineva, M. A.; Mahilum-Tapay, L.; Lee, H. Sample preparation: a challenge in the development of point-of-care nucleic acid-based assays for resource-limited settings. *Analyst* **2007**, *132*, 1193−1199.
(38) Lee, C. Y.; Chang, C. L.; Wang, Y. N.; Fu, L. M. Microfluidic mixing: a review. *Int. J. Mol. Sci.* **2011**, *12*, 3263−3287.
(39) Gao, L.; McCarthy, T. J. Contact angle hysteresis explained. *Langmuir* **2006**, *22*, 6234−6237.
(40) Clark, J.; Kaufman, M.; Fodor, P. S. Mixing Enhancement in Serpentine Micromixers with a Non-Rectangular Cross-Section. *Micromachines* **2018**, *9*, No. 107.
(41) Modak, S. S.; Barber, C. A.; Geva, E.; Abrams, W. R.; Malamud, D.; Ongagna, Y. S. Y. Rapid Point-of-Care Isothermal Amplification Assay for the Detection of Malaria without Nucleic Acid Purification. *Infect. Dis.* **2016**, *9*, 1−9.
(42) Hardinge, P.; Murray, J. A. H. Full Dynamic Range Quantification using Loop-mediated Amplification (LAMP) by Combining Analysis of Amplification Timing and Variance between Replicates at Low Copy Number. *Sci. Rep.* **2020**, *10*, No. 916.
(43) Perandin, F.; Manca, N.; Calderaro, A.; Piccolo, G.; Galati, L.; Ricci, L.; Medici, M.; Arcangeletti, M.; Snounou, G.; Dettori, G.; Chezzi, C. Development of a real-time PCR assay for detection of *Plasmodium falciparum*, *Plasmodium vivax*, and *Plasmodium ovale* for routine clinical diagnosis. *J. Clin. Microbiol.* **2004**, *42*, 1214−1219.
(44) Polley, S. D.; Mori, Y.; Watson, J.; Perkins, M. D.; González, I. J.; Notomi, T.; Chiodini, P. L.; Sutherland, C. J. Mitochondrial DNA targets increase sensitivity of malaria detection using loop-mediated isothermal amplification. *J. Clin. Microbiol.* **2010**, *48*, 2866−2871.
(45) Choi, G.; Song, D.; Shrestha, S.; Miao, J.; Cui, L.; Guan, W. A field-deployable mobile molecular diagnostic system for malaria at the point of need. *Lab Chip* **2016**, *16*, 4341−4349.
(46) He, X.; Tang, Z.; Liang, S.; Liu, M.; Guan, W. Confocal scanning photoluminescence for mapping electron and photon beam-induced microscopic changes in SiNx during nanopore fabrication. *Nanotechnology* **2020**, *31*, No. 395202.

https://doi.org/10.1021/acssensors.2c02169
ACS Sens. 2023, 8, 673−683